Обзор ArXiv/astro-ph, 7-12 ноября 2019 года

От Сильченко О.К.

ArXiv: 1911.02087

Planck evidence for a closed Universe and a possible crisis for cosmology

Eleonora Di Valentino[1], Alessandro Melchiorri[2], Joseph Silk[3,4,5,6]

The recent Planck Legacy 2018 release has confirmed the presence of an enhanced lensing amplitude in CMB power spectra compared to that predicted in the standard ΛCDM model. A closed universe can provide a physical explanation for this effect, with the Planck CMB spectra now preferring a positive curvature at more than 99% C.L. Here we further investigate the evidence for a closed universe from Planck, showing that positive curvature naturally explains the anomalous lensing amplitude and demonstrating that it also removes a well-known tension within the Planck data set concerning the values of cosmological parameters derived at different angular scales. We show that since the Planck power spectra prefer a closed universe, discordances higher than generally estimated arise for most of the local cosmological

Вселенная замкнута по данным Planck 2018

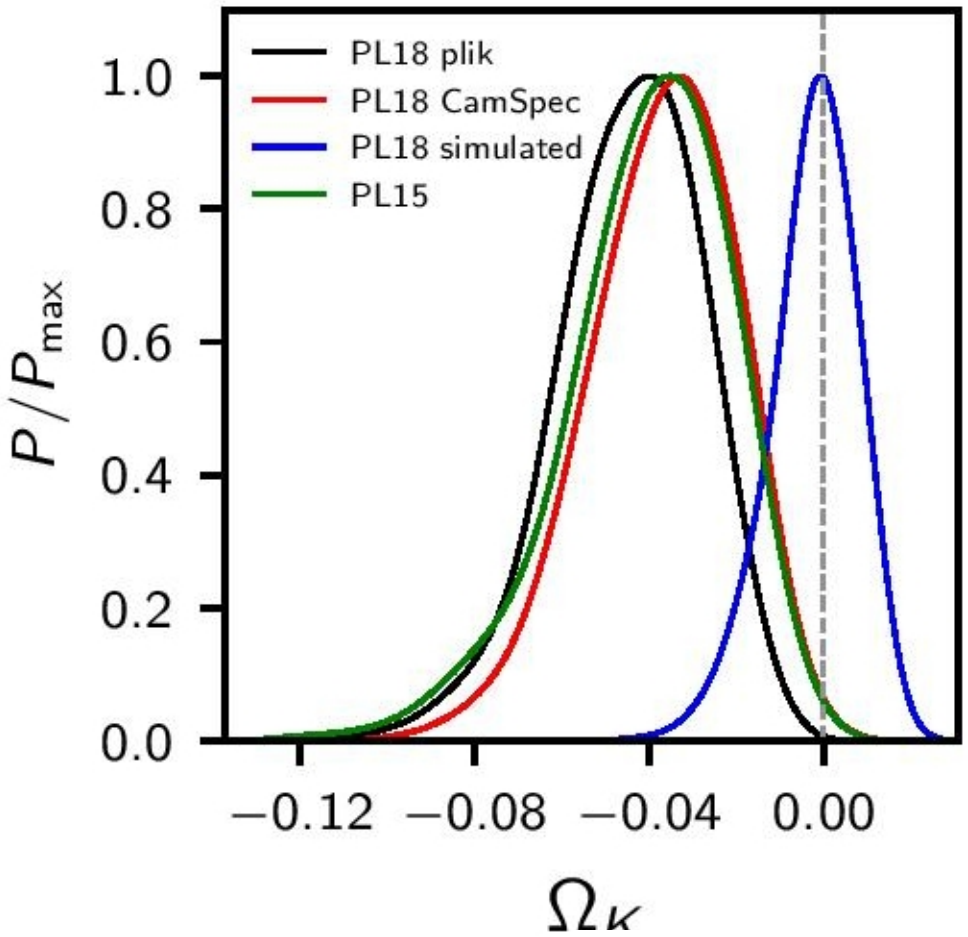

universe. The constraints from the PL18 CMB spectra on curvature, parameterized through the energy density parameter Ω_K, are indeed quite surprising, suggesting a closed universe at 3.4 standard deviations ($-0.007 > \Omega_K > -0.095$ at 99% C.L. [1–3]).

Это стало очевидным при выходе Planck на высокие пространственные частоты, где уже заиграло линзирование реликтового фона

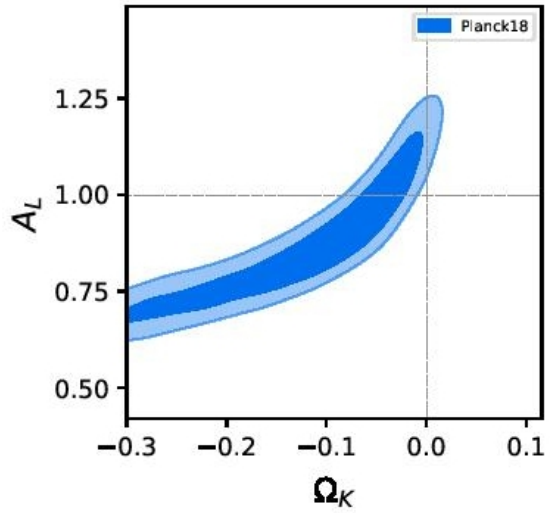

Figure 2: **Degeneracy between curvature and lensing**. Constraints at 68% and 95% in the A_{lens} vs Ω_K plane from Planck 2018 temperature and polarization data. A degeneracy between curvature and the A_{lens} parameter is clearly present. Note that a model with $\Omega_K < 0$ is slightly preferred with respect to a flat model with $A_{lens} > 1$.

Если согласиться на замкнутую Вселенную, то космологические параметры будут определяться одинаково по высоким и низким пространственным частотам

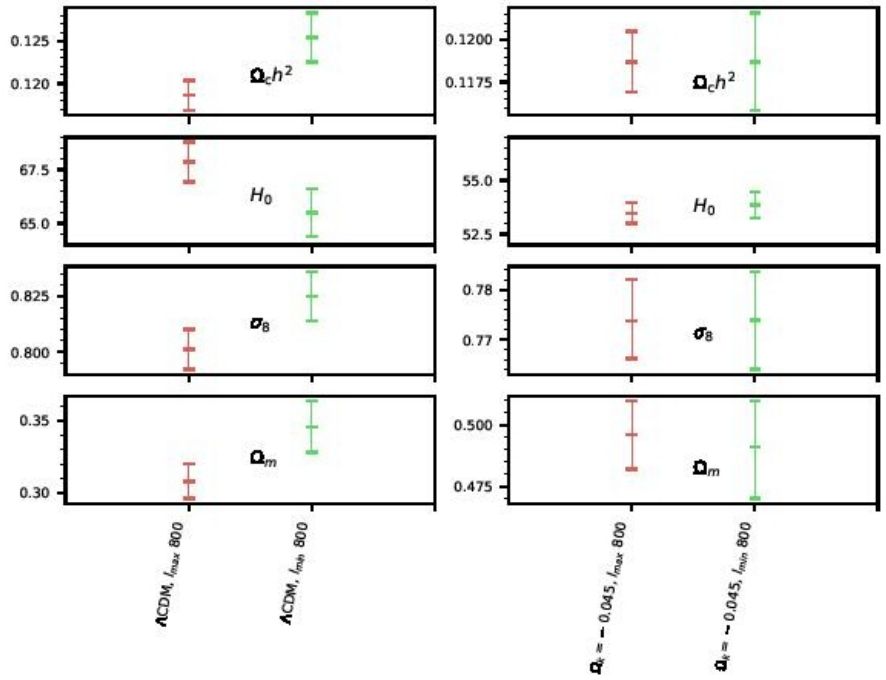

Figure 3: **Curvature and parameters shift**. Cosmological parameters derived from two different multipoles ranges ($2 \leq \ell \leq 800$ and $800 < \ell \leq 2500$) of the Planck 2018 temperature and polarization data assuming either a ΛCDM model (Left) or a closed model (Right). Polarization

…но зато окончательно располземся сравнение с ближней (вплоть до z=3) Вселенной

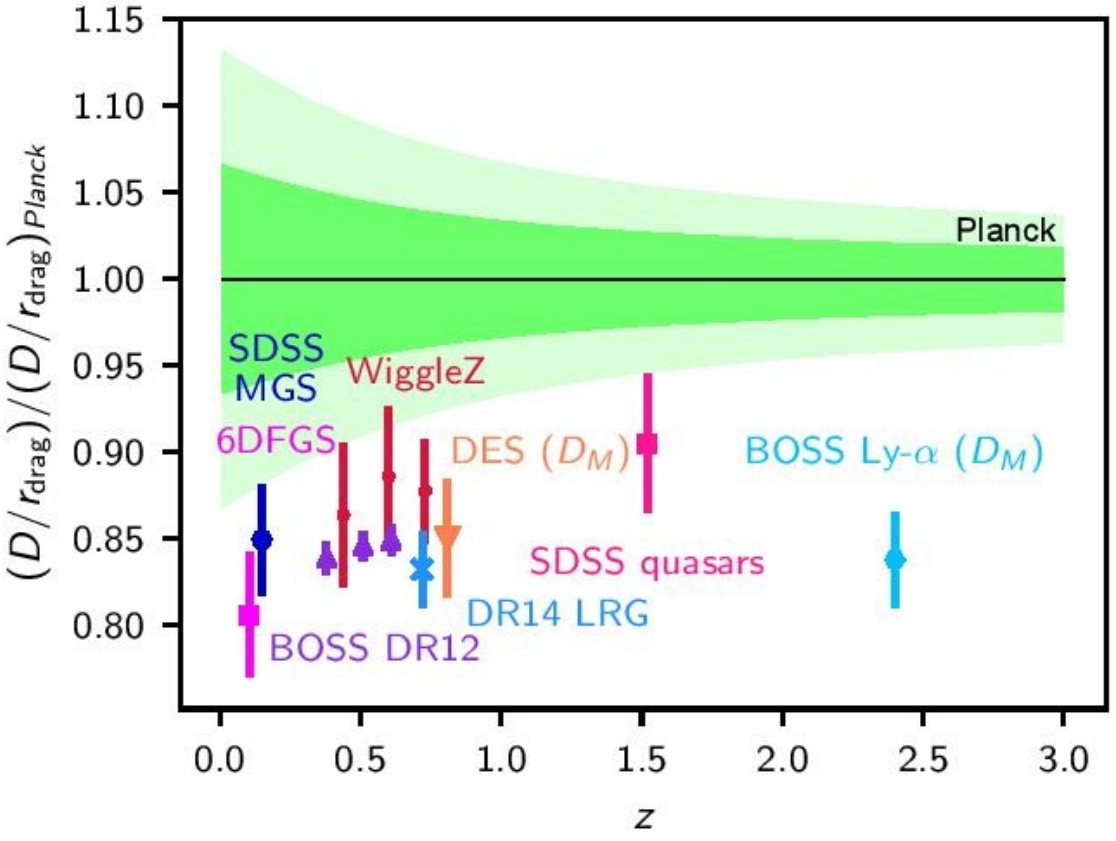

…но зато окончательно расползется сравнение с ближней (вплоть до z=3) Вселенной

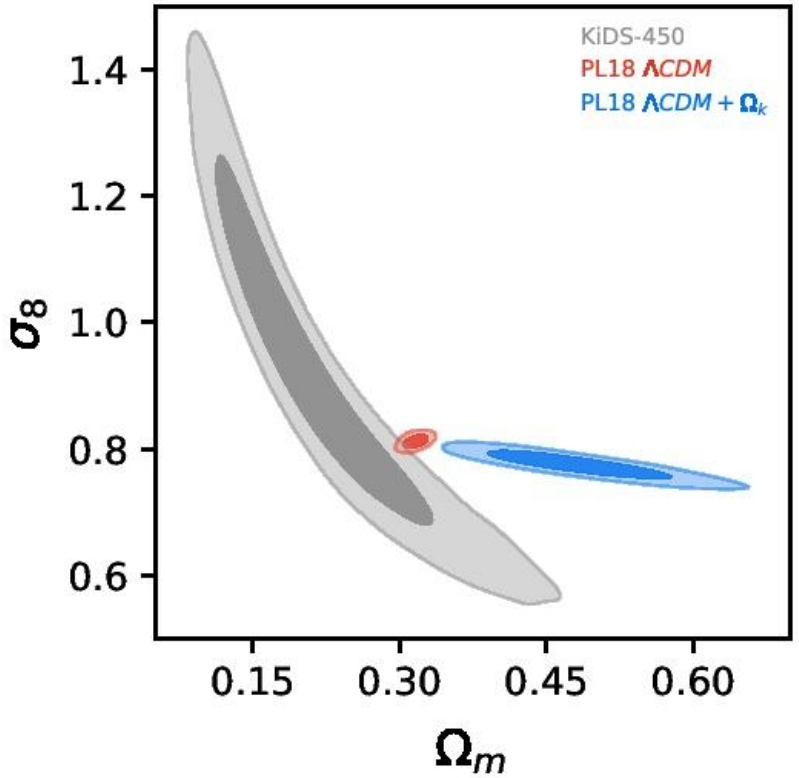

Figure 6: **Tension with cosmic shear measurements**. Discordance between PL18 and the

…но зато окончательно расползется сравнение с ближней (вплоть до z=3) Вселенной

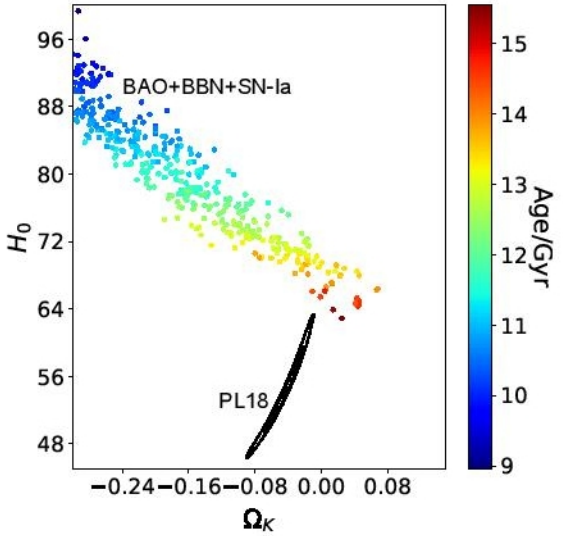

Figure 7: **Tension with combined data**. Contour plots at 68% and 95% C.L. from PL18 and

И с постоянной Хаббла станет еще хуже!

ArXiv: 1911.03717

Geometric properties of galactic discs with clumpy episodes

Leandro Beraldo e Silva[1]★, Victor P. Debattista[1], Tigran Khachaturyants[1], David Nidever[2], Kathryn Johnston[3]

[1] *Jeremiah Horrocks Institute, University of Central Lancashire, Preston, PR1 2HE, UK*
[2] *Department of Physics, Montana State University, P.O. Box 173840, Bozeman, MT 59717-3840, USA*
[3] *National Optical Astronomy Observatory, 950 North Cherry Ave, Tucson, AZ 85719, USA*

Accepted XXX. Received YYY; in original form ZZZ

ABSTRACT

A scenario for the formation of the bi-modality in the chemical space [α/Fe] vs [Fe/H] of the Milky Way was recently proposed in which α-enhanced stars are produced early and quickly in clumps. Besides accelerating the enrichment of the medium with α-elements, these clumps scatter the old stars, converting in-plane to vertical motion, forming a geometric thick disc. In this paper, by means of a detailed analysis of the data from smooth particle hydrodynamical simulations, we investigate the geometric properties (in particular of the chemical thick disc) produced in this scenario. For mono-age populations we show that the surface radial density profiles of high-[α/Fe] stars are well described by single exponentials, while that of low-[α/Fe] stars require broken exponentials. This break is sharp for young populations and broadens for older ones. The position of the break does not depend significantly on age. The vertical density profiles of mono-age populations are characterized by single exponentials, which flare significantly for low-[α/Fe] stars but only weakly (or not at all) for high-[α/Fe] stars. For low-[α/Fe] stars, the flaring level decreases with age, while for high-[α/Fe] stars it weakly increases with age (although with large uncertainties). All these properties are in agreement with observational results recently reported for the Milky Way, making this a plausible scenario for the formation of the Galactic thick disc.

Модели

$\nu_\star(R,z\|\theta) = \Sigma(R\|\theta)\rho(z\|R,\theta)$	$\rho(z\|R,\theta)$	$\Sigma(R\|\theta)$
M1	double exp., Eq. (4)	single exp., Eq. (2)
M2	single exp., Eq. (5)	
M3	single flaring exp., Eqs. (5) and (6)	
M4	double fl. inner exp., Eqs. (4) and (6)	
M5	single flaring exp., Eqs. (5) and (6)	broken exp., Eq. (7)

Table 1. Summary of models fitted to the simulation data.

Это все звезды, если есть клампы

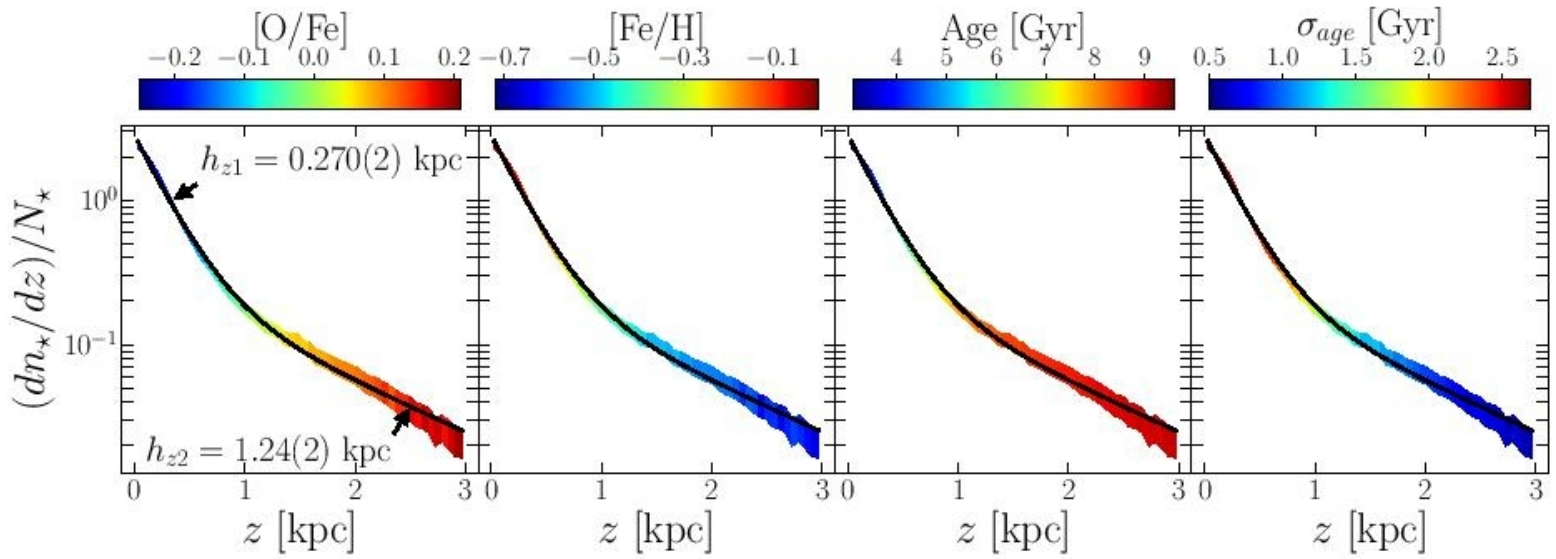

Figure 1. Density profile of the complete sample of star particles in the Solar neighborhood $6 < R < 10$ kpc, $|z| < 3$ kpc. From left to right, the plots are colour-coded by [O/Fe], [Fe/H], age and age dispersion, respectively. Similarly to the MW (see Jurić et al. 2008), the data are well described by a double exponential model defining the geometric thin and thick discs, with scale height values shown in the left panel. The thick component ($|z| \gtrsim 1$kpc) is characterized by α-rich, metal-poor and old populations, while the thin component ($|z| \lesssim 1$kpc) is α-poor, metal-rich, young on average but with large age dispersions.

Это все звезды, если нет клампов

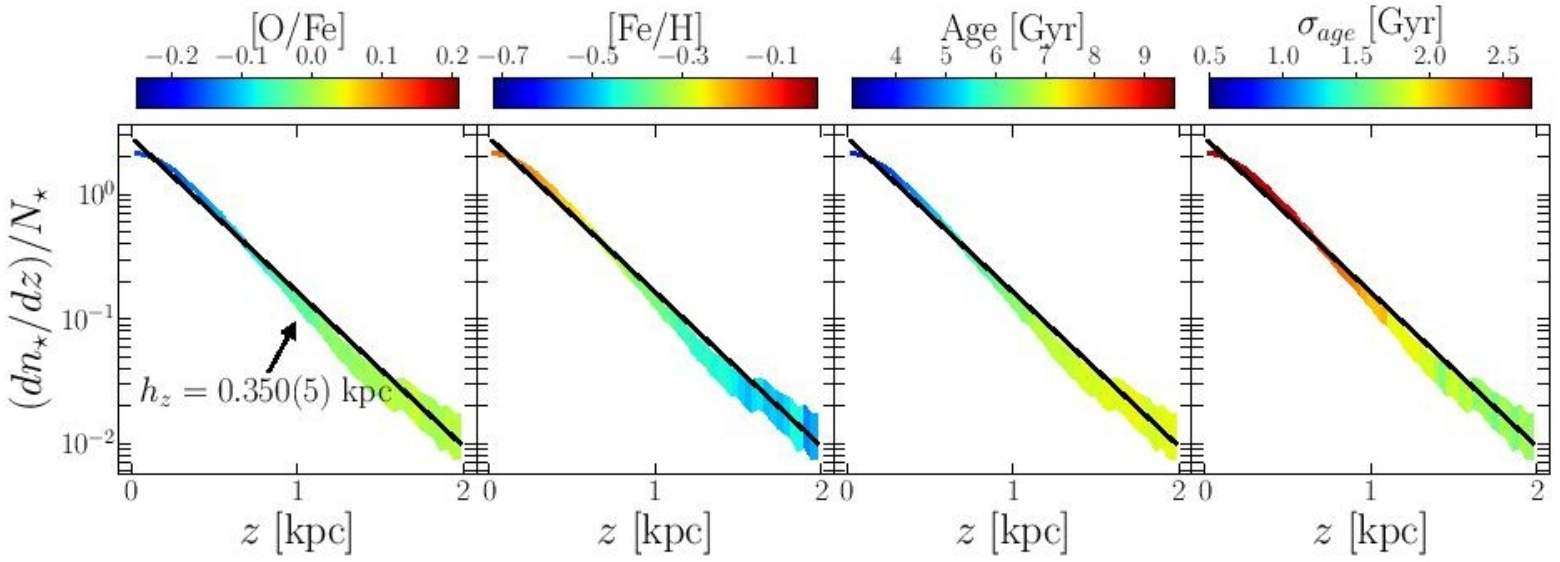

Figure 2. Density profile of the complete sample of star particles in the Solar neighborhood $6 < R < 10$ kpc, $|z| < 3$ kpc for the simulation **FB80**. From left to right, the plots are colour-coded by [O/Fe], [Fe/H], age and age dispersion, respectively. We see that the data is described by a single exponential (black line), i.e., different from the MW, with no geometric thick disc.

Это моно-химические населения

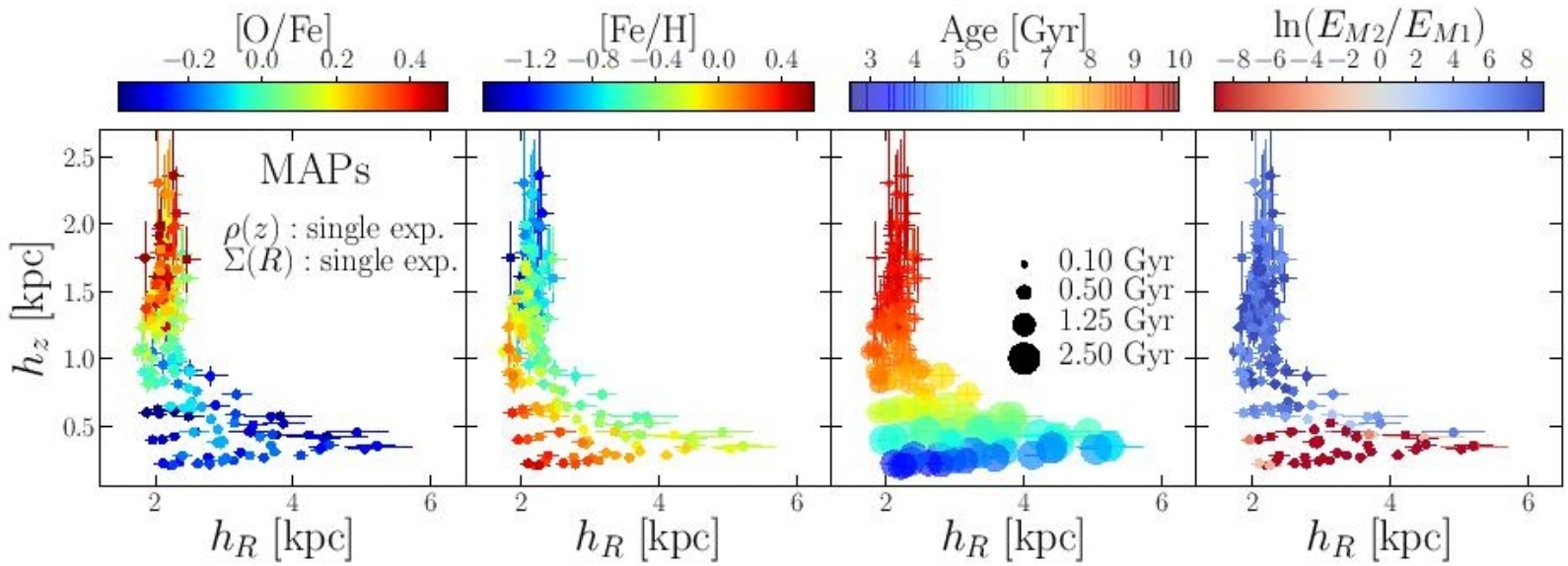

Figure 3. Best fit values of radial scale length h_R vs vertical scale height h_z for mono-abundance populations of star particles in $5 < R < 12$ kpc, $0.3 < |z| < 3$ kpc. From left to right, panels are colour-coded by [O/Fe], [Fe/H], mean age (point sizes meaning age dispersion) and by the Bayes factor comparing the fit quality of single vs double exponentials for the vertical density profile –see Eqs. (9)-(10). In agreement with Bovy et al. (2012), α-rich and metal-poor MAPs are thick and centrally concentrated, as opposed to α-poor and metal-rich MAPs, which are thin and spread out in radius. MAPs with older stars are more uniform in age and have vertical profiles better fitted by single exponentials, while younger MAPs have broader age distributions and are better fitted by double exponentials.

Это моно-возрастные населения

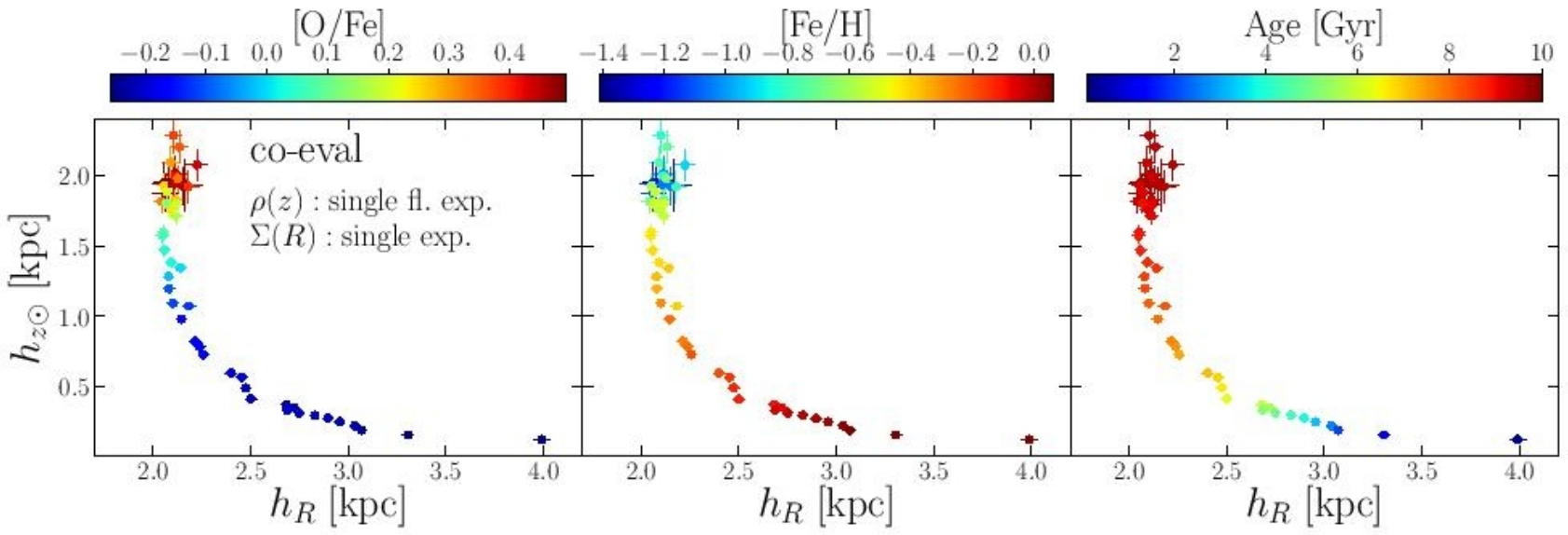

Figure 4. Best fit values of radial scale length h_R vs vertical scale height at the Solar position $h_{z\odot}$ for mono-age populations obtained fitting a single flaring exponential model. Star particles are selected in $5 < R < 12$ kpc, $|z| < 3$ kpc. The anti-correlation between h_R and $h_{z\odot}$ and the trends with [O/Fe], [Fe/H] and age are similar to, but cleaner than, those for MAPs – Fig. 3.

Тонкие диски всегда обрезанные!

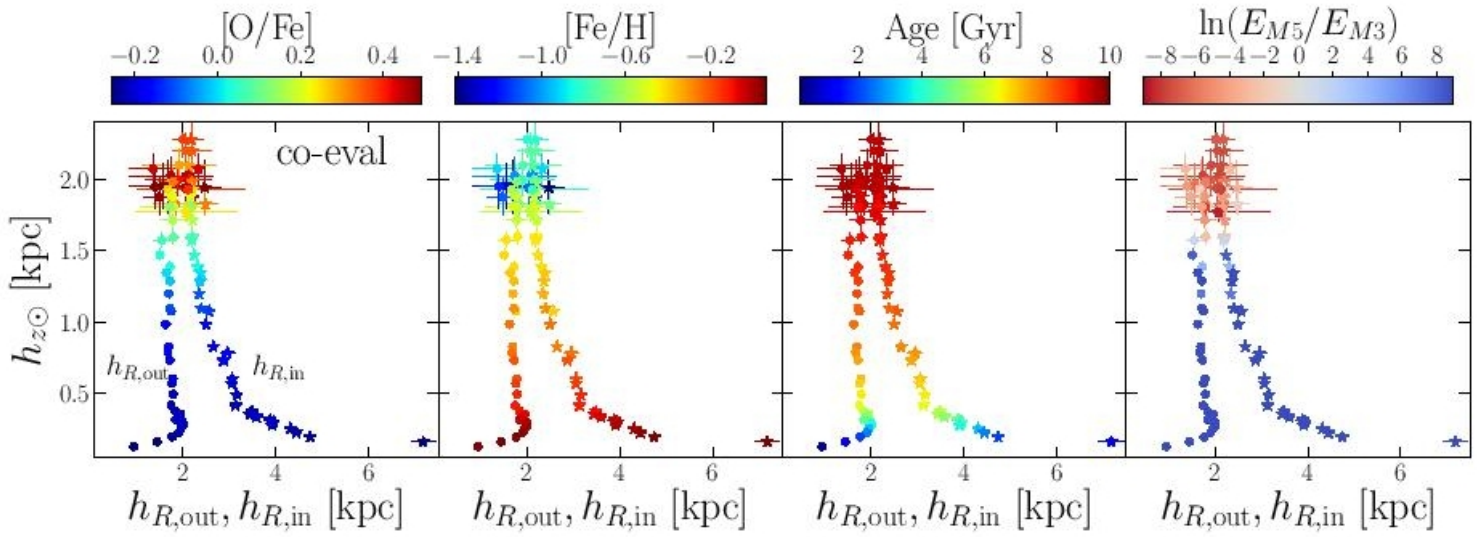

Figure 6. Best fit values of the outer and inner radial scale lengths $h_{R,\mathrm{out}}$, $h_{R,\mathrm{in}}$ vs vertical scale height at the Solar position $h_{z\odot}$ for mono-age populations obtained fitting a single flaring exponential model for $\rho(z|R)$ and a broken exponential for $\Sigma(R)$ – model **M5**. The data selection, model fit and colour-coding are the same as that of Fig. 4. Young, α-poor and metal-rich populations have sharp breaks, i.e. significant differences $h_{R,\mathrm{in}} - h_{R,\mathrm{out}}$, while old, α-rich, metal-poor populations have $h_{R,\mathrm{out}} \approx h_{R,\mathrm{in}}$, and thus flat exponential profiles. The right panel is colour-coded by the Bayes factor comparing the single versus broken exponential models for $\Sigma(R)$. High-[O/Fe] populations are better described by single exponentials (red points), while low [O/Fe] populations strongly favour the broken exponential model (blue points).

И обрыв стоит на месте!

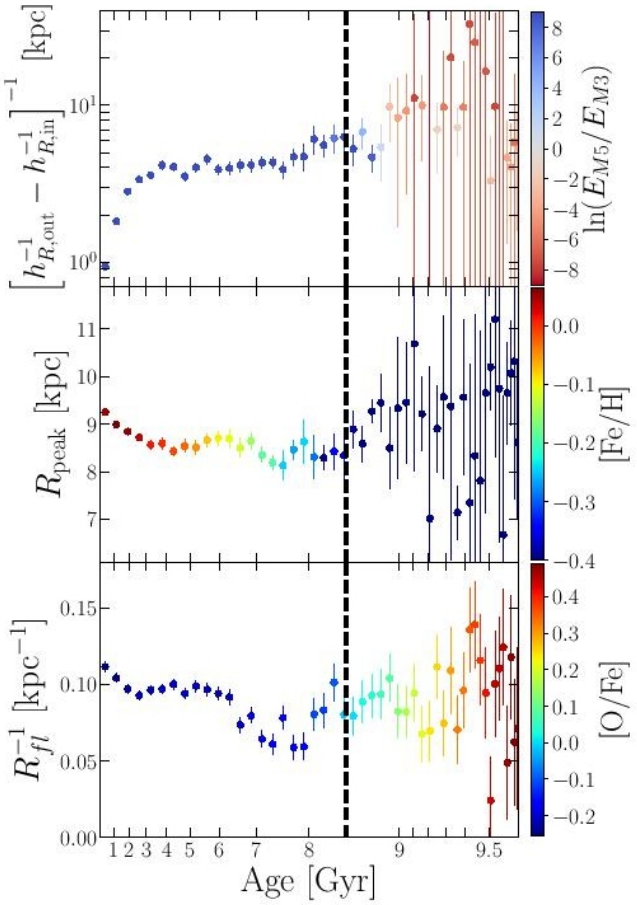

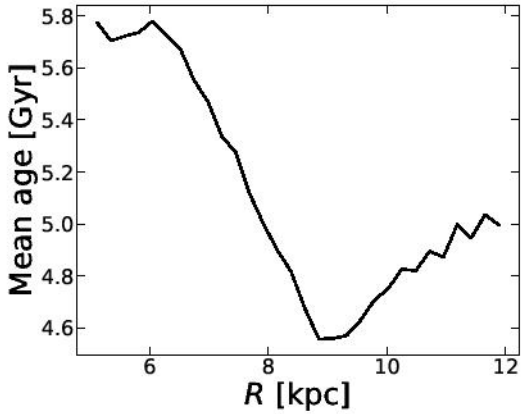

Figure 8. The mean stellar age at each radius obtained with the simulation **FB10**. As found by Roškar et al. (2008), the position of the minimum, here at $R \approx 9$ kpc, correlates well with the position of the break in $\Sigma(R)$ for the youngest population, shown in the central panel of Fig. 7.

Их первая статья на эту тему

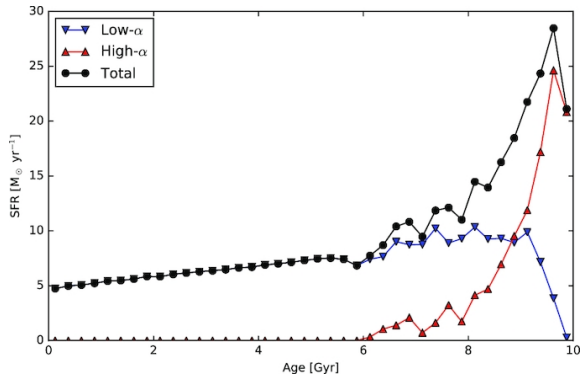

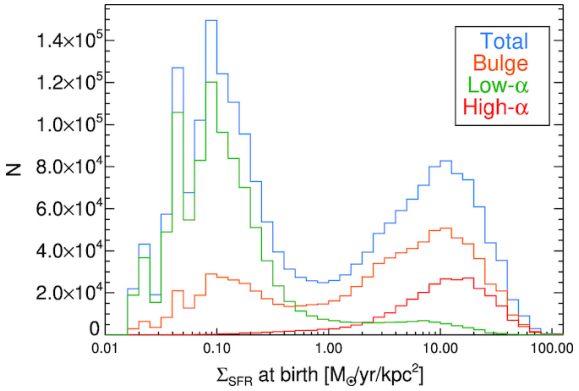

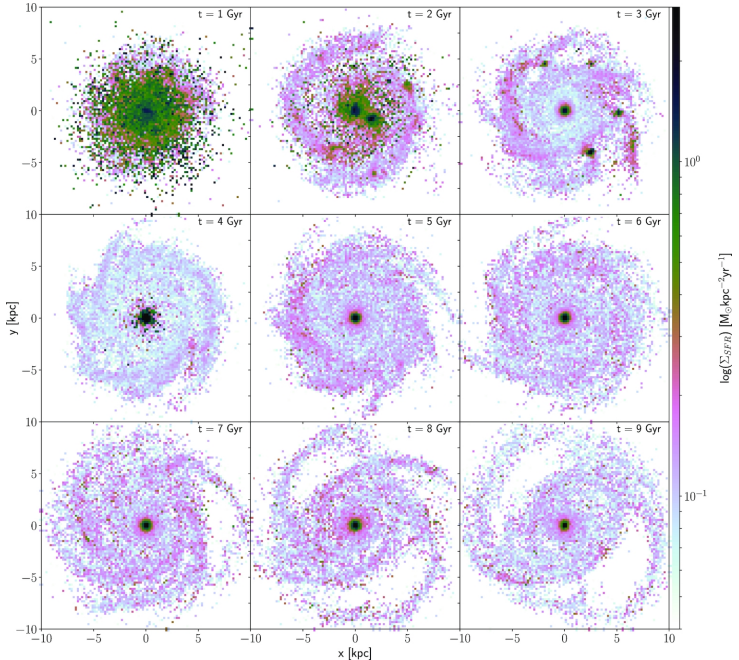

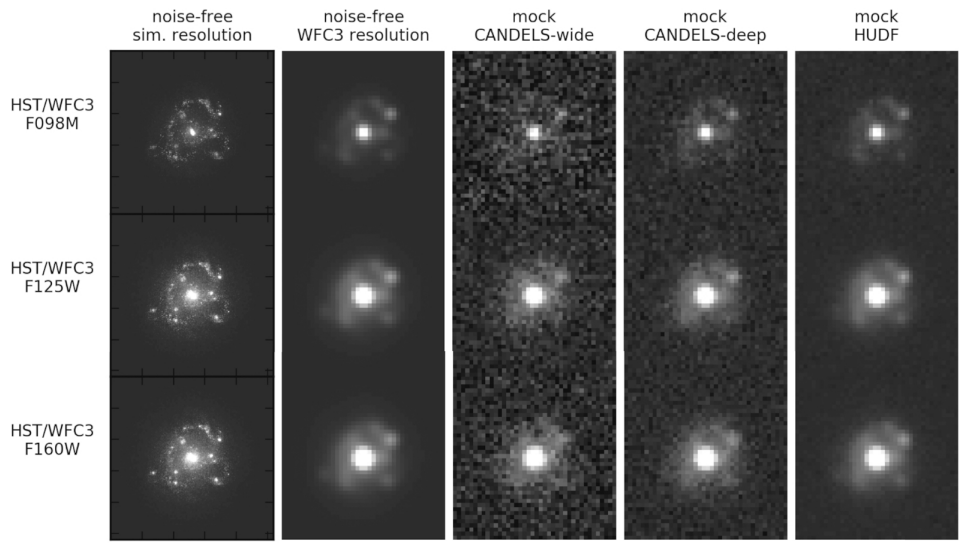

ArXiv: 1911.03702

The initial mass function in the extended ultraviolet disk of M83

S. M. Bruzzese[1], David A. Thilker[2], G. R. Meurer[1], Luciana Bianchi[2], A. B. Watts[1], A. M. N. Ferguson[3], A. Gil de Paz[4], B. Madore[5,6], D. Christopher Martin[7], and R. Michael Rich[8]

[1] *International Centre for Radio Astronomy Research, The University of Western Australia, Crawley, WA, Australia*
[2] *Department of Physics and Astronomy, The Johns Hopkins University, Baltimore, MD, USA*
[3] *Institute for Astronomy, Royal Observatory Edinburgh, University of Edinburgh, Blackford Hill, Edinburgh EH9 3HJ, United Kingdom*
[4] *Departamento de Física de la Tierra y Astrofísica, Universidad Complutense de Madrid, E-28040 Madrid, Spain*
[5] *Department of Astronomy & Astrophysics, University of Chicago, 5640 South Ellis Avenue, Chicago, IL 60637, USA*
[6] *Observatories of the Carnegie Institution for Science, 813 Santa Barbara Street, Pasadena, CA 91101, USA*
[7] *California Institute of Technology, Pasadena, CA 91125, USA*
[8] *Department of Physics and Astronomy, UCLA, Los Angeles, California 90095-1547*

13 November 2019

ABSTRACT

Using *Hubble Space Telescope* ACS/WFC data we present the photometry and spatial distribution of resolved stellar populations of four fields within the extended ultraviolet disk (XUV disk) of M83. These observations show a clumpy distribution of main-sequence stars and a mostly smooth distribution of red giant branch stars. We constrain the upper-end of the initial mass function (IMF) in the outer disk using the detected population of main-sequence stars and an assumed constant star formation rate (SFR) over the last 300 Myr. By comparing the observed main-sequence lumi-

Figure 1. Colour image of M83 composed of H I Very Large Array (red), NUV GALEX (green), and FUV GALEX (blue) data. This combination results in the strongly star forming central region to appear as a combination of white, cyan, and pink tones, while the outer disk is dominated by the H I arms/filaments appearing in red, dotted in blue revealing the XUV disk star forming complexes. The position of the four ACS/WFC fields are labelled and shown as white footprints. The short line segments in each footprint mark a portion of the divide between the two

Диаграмма цвет-светимость для звезд: глав. Посл. И ветвь гигантов

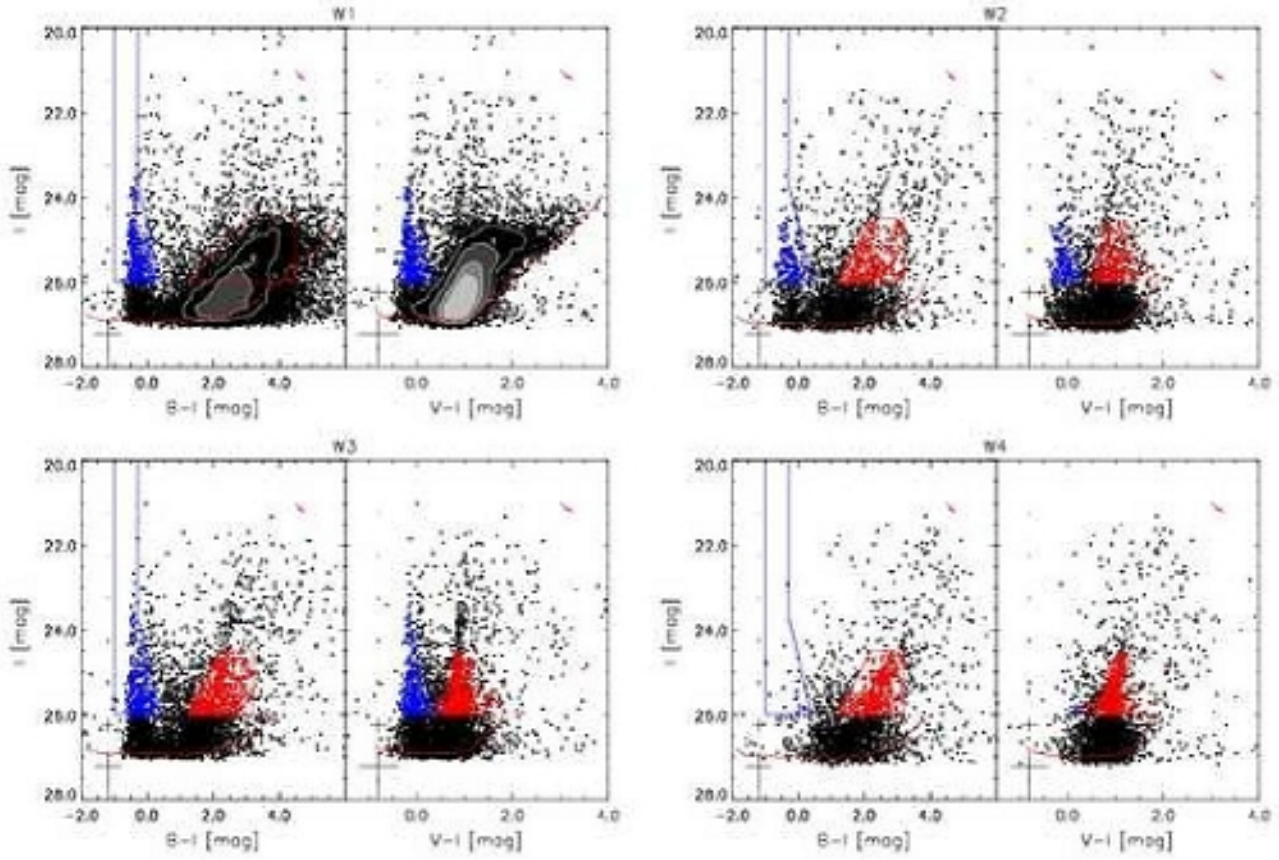

Figure 4. CMDs of the ACS/WFC data in I versus $(B\text{-}I)$ (left) and I versus $(V\text{-}I)$ (right) for each of the individual HST fields. Polygon boxes, identical for each field, are shown in the $(B\text{-}I)$ CMDs, and are used to select stellar evolutionary phases; the blue polygon identifies MS stars, while the red polygon identifies RGB stars. Stellar sources in these boxes are shown as blue and red dots respectively. Contours are used in the saturated portion of the colour-magnitude diagrams, calculated using bins 0.2 mag wide in both colour and magnitude, and contour levels at 50, 100, 200, and 300 stars per bin in each panel. Uncertainties derived from the artificial star tests are shown as error bars on the left side of the panels. The 60% completeness limits are shown as thick red lines and the red arrows indicate assumed foreground dust extinction.

Пересчитали звезды: Солпитеровская НФМ с обрезанным верхом

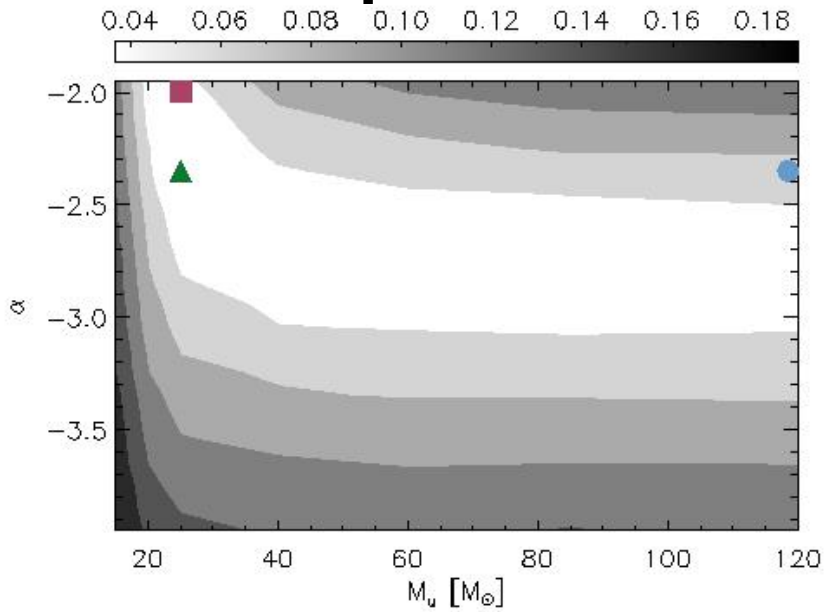

Figure 11. Contour plot showing the mean test statistic, d, for the IMF slope α and upper-mass limit M_u for the combined MSLF IMF analysis. The best-fitting IMF parameters (where d is minimised) are shown as a filled olive-green triangle. There is however, little difference between the best-fitting parameters and the elongated minimum region shown in white. The Kroupa IMF parameters are indicated with a pale-blue filled circle, while the best-fitting IMF parameters that match the Hα constraints are indicated with a brick-red filled square. These latter two symbols have been shifted slightly from their nominal positions at the edge of the parameter space so as to be clearly visible in the figure.

И это уже не первый результат такого рода для внешних дисков!

Table 9. Best-fitting IMF parameters for the outer disks of NGC 2915, DDO 154 and M83. The standard IMF parameters of a Kroupa IMF are included for comparison.

Galaxy	α	$M_u\,(M_\odot)$	reference
M83	-2.35	25	This study
NGC 2915	-2.85	60	B15
DDO 154	-2.45	16	Watts et al. (2018)
Kroupa	-2.35	120	Kroupa (2001)